Supporting Information for:

Narrowing the band of green emission in manganese hybrid by reducing the hydrogen bond strength and structural distortion

Jiawei Lin,[a] Muwei Zhang,[a] Niu Sun,[a] Shihui He,[b] Xusheng Zhang,[b] Zhongnan Guo,[*a] Jing Zhao,[b] Quanlin Liu,[b] and Wenxia Yuan,[*a]

[a] Department of Chemistry, School of Chemistry and Biological Engineering, University of Science and Technology Beijing, Beijing, 100083, China

[b] The Beijing Municipal Key Laboratory of New Energy Materials and Technologies, School of Materials Sciences and Engineering, University of Science and Technology Beijing, Beijing, 100083, China

CONTENTS

Table S1. Crystal data and structure refinement of $(MDPA)_2MnBr_4$ and $(MTPP)_2MnBr_4$. S3

Figure S1. ORTEP plots for (a) $(MDPA)_2MnBr_4$ and (b) $(MTPP)_2MnBr_4$. S5

Figure S2. The EDS analysis results for (a) $(MDPA)_2MnBr_4$ and (b) $(MTPP)_2MnBr_4$. S5

Figure S3. Mn-Br bond lengths of $[MnBr_4]^{2-}$ in $(MDPA)_2MnBr_4$ and $(MTPP)_2MnBr_4$. S5

Figure S4. The coordinates of $(MDPA)_2MnBr_4$, $(MTPP)_2MnBr_4$ and NTSC-green standard in CIE 1931 system. S6

Figure S5. PLQYs of $(MDPA)_2MnBr_4$ and $(MTPP)_2MnBr_4$. S6

Figure S6. Comparison of the PL spectra of the as-prepared (a) $(MDPA)_2MnBr_4$ and (b) $(MTPP)_2MnBr_4$ and the ones of samples exposed in the air for 1 month. S7

Figure S7. Relationship between the fwhm values and the bond angle distortion degree (δ_{tet}^2) in 0D Mn(II) tetrabromide hybrids. S7

Figure S8. The thermal activation energy ΔE of (a) $(MDPA)_2MnBr_4$ and (b) $(MTPP)_2MnBr_4$ analyzed by using the Arrhenius equation. S7

Figure S9. Temperature-dependent PL decay curves and lifetimes of (a) $(MDPA)_2MnBr_4$ and (b) $(MTPP)_2MnBr_4$. S8

Figure S10. Photographs of the TL light captured from crystals of $(MDPA)_2MnBr_4$ (left) and $(MTPP)_2MnBr_4$ (right) upon grinding with a glass rod at ambient conditions. S8

Table S1. Crystal data and structure refinement of $(MDPA)_2MnBr_4$ and $(MTPP)_2MnBr_4$.

Empirical formula	$(C_{13}H_{14}N)_2MnBr_4$	$(C_{19}H_{18}N)_2MnBr_4$
Formula weight	743.08	929.19
Temperature	150.0 K	
Wavelength	0.71073 Å	
Crystal system	triclinic	monoclinic
Space group	$P1$	$P2_1$
Unit cell dimensions	a = 8.3674(4) Å, α = 87.103(2)°	a = 9.7629(6) Å, α = 90°
	b = 8.5704(4) Å, β = 67.081(2)°	b = 12.4204(6) Å, β = 105.027(2)°
	c = 10.6100(5) Å, γ = 86.628(2)°	c = 16.5351(10) Å, γ = 90°
Volume	699.27(6) Å^3	1936.47(19) Å^3
Z	1	2
Density (calculated)	1.765 g/cm^3	1.594 g/cm^3
Absorption coefficient	6.203 mm^{-1}	4.575 mm^{-1}
F(000)	363	918
Crystal size	0.22×0.18×0.18 mm^3	0.15×0.15×0.12 mm^3
θ range for data collection	3.213 to 26.426°	2.077 to 26.394°
Index ranges	$-10 \le h \le 10$	$-12 \le h \le 12$
	$-10 \le k \le 10$	$-15 \le k \le 15$
	$-13 \le l \le 13$	$-20 \le l \le 20$
Reflections collected	16228	22338
Independent reflections	5619 [Rint = 0.0261]	7870 [Rint = 0.0402]
Completeness	98.1%	99.9%
Refinement method	Full-matrix least-squares on F^2	
Data / restraints / parameters	5619/3/289	7870/1/408
Goodness-of-fit	1.054	0.910
Flack factor	0.043(13)	0.013(6)
Final R indices [$I > 2\sigma(I)$]	R_{obs} = 0.0302, wR_{obs} = 0.0727	R_{obs} = 0.0320, wR_{obs} = 0.0517
R indices [all data]	R_{all} = 0.0341, wR_{all} = 0.0740	R_{all} = 0.0507, wR_{all} = 0.0563
Largest diff. peak and hole	0.708 and -0.413 e·Å^{-3}	0.320 and -0.267 e·Å^{-3}

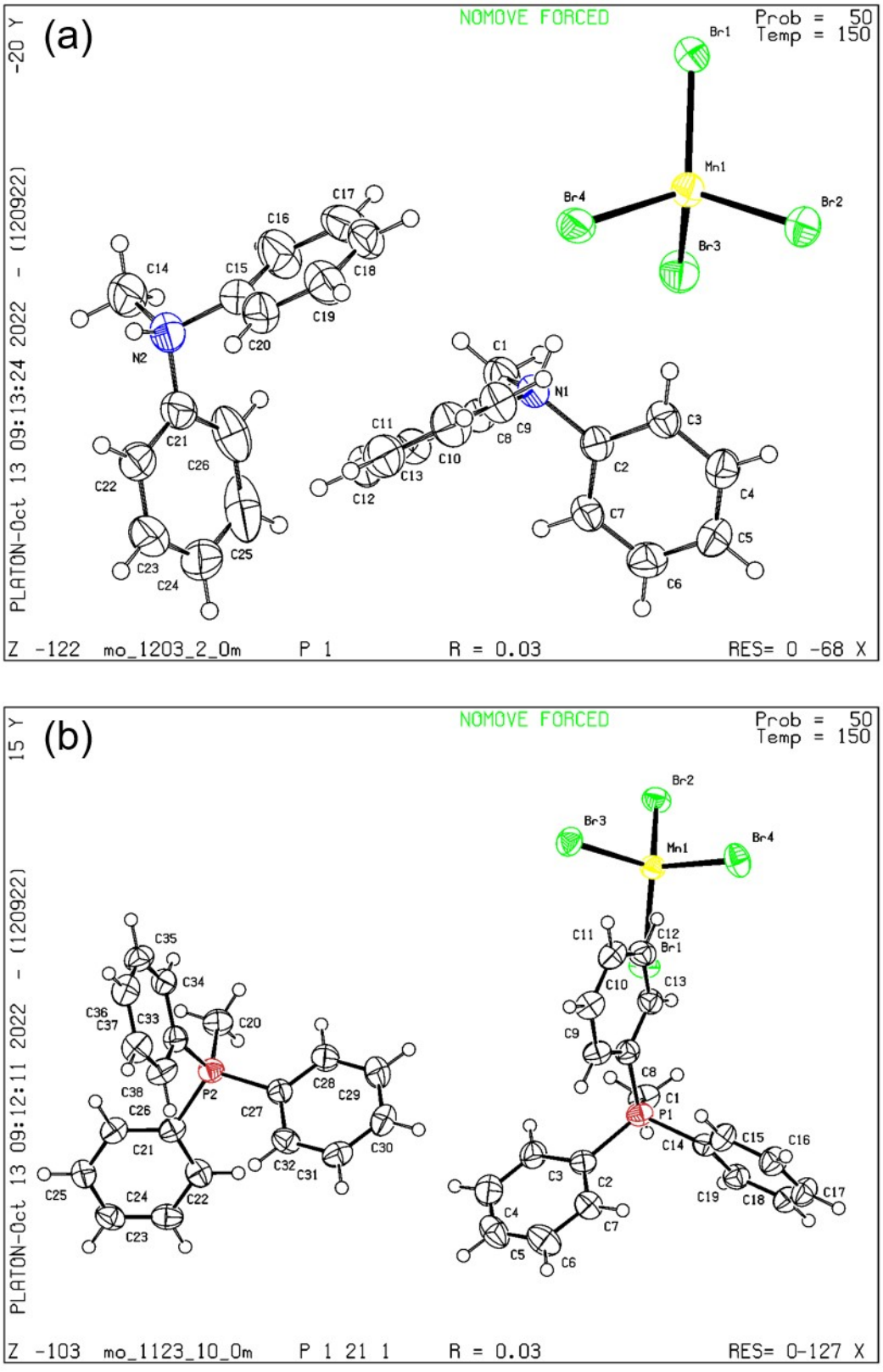

Figure S1. Oak Ridge thermal ellipsoid plots (ORTEP) for (a) $(MDPA)_2MnBr_4$ and (b) $(MTPP)_2MnBr_4$.

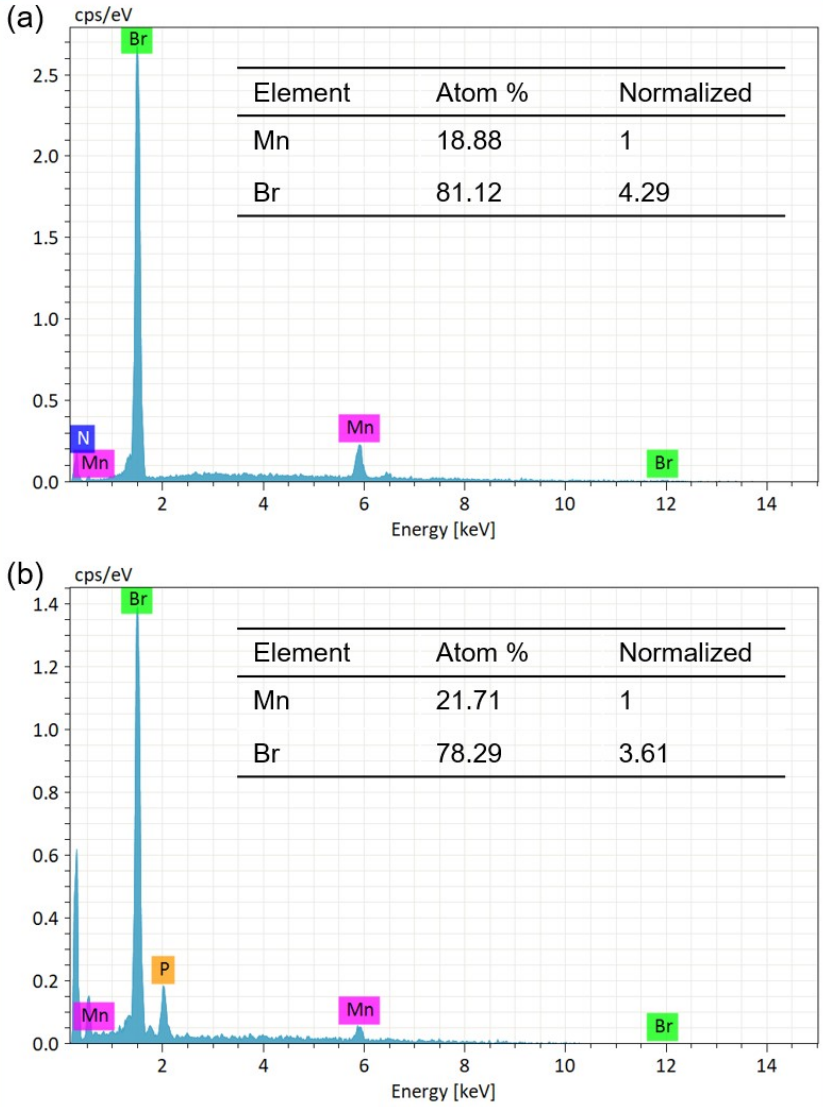

Figure S2. Element analysis results via EDS for (a) $(MDPA)_2MnBr_4$ and (b) $(MTPP)_2MnBr_4$.

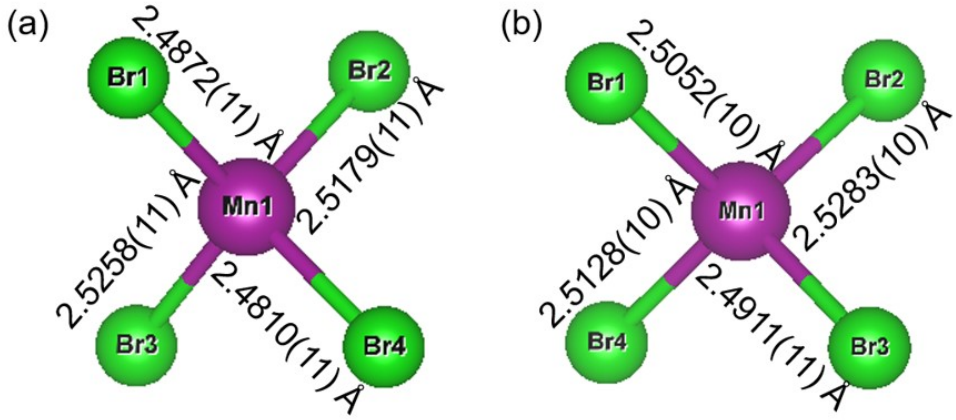

Figure S3. Mn-Br bond lengths of $[MnBr_4]^{2-}$ in (a) $(MDPA)_2MnBr_4$ and (b) $(MTPP)_2MnBr_4$.

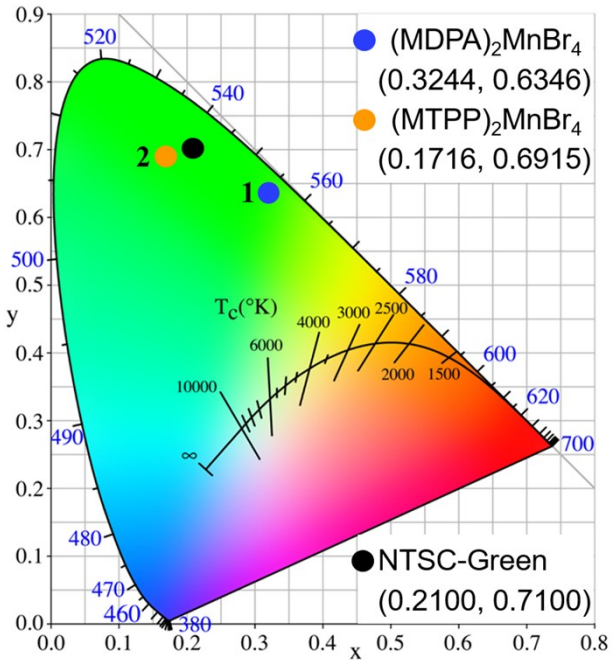

Figure S4. The coordinates of $(MDPA)_2MnBr_4$, $(MTPP)_2MnBr_4$ and NTSC-green standard in CIE 1931 system.

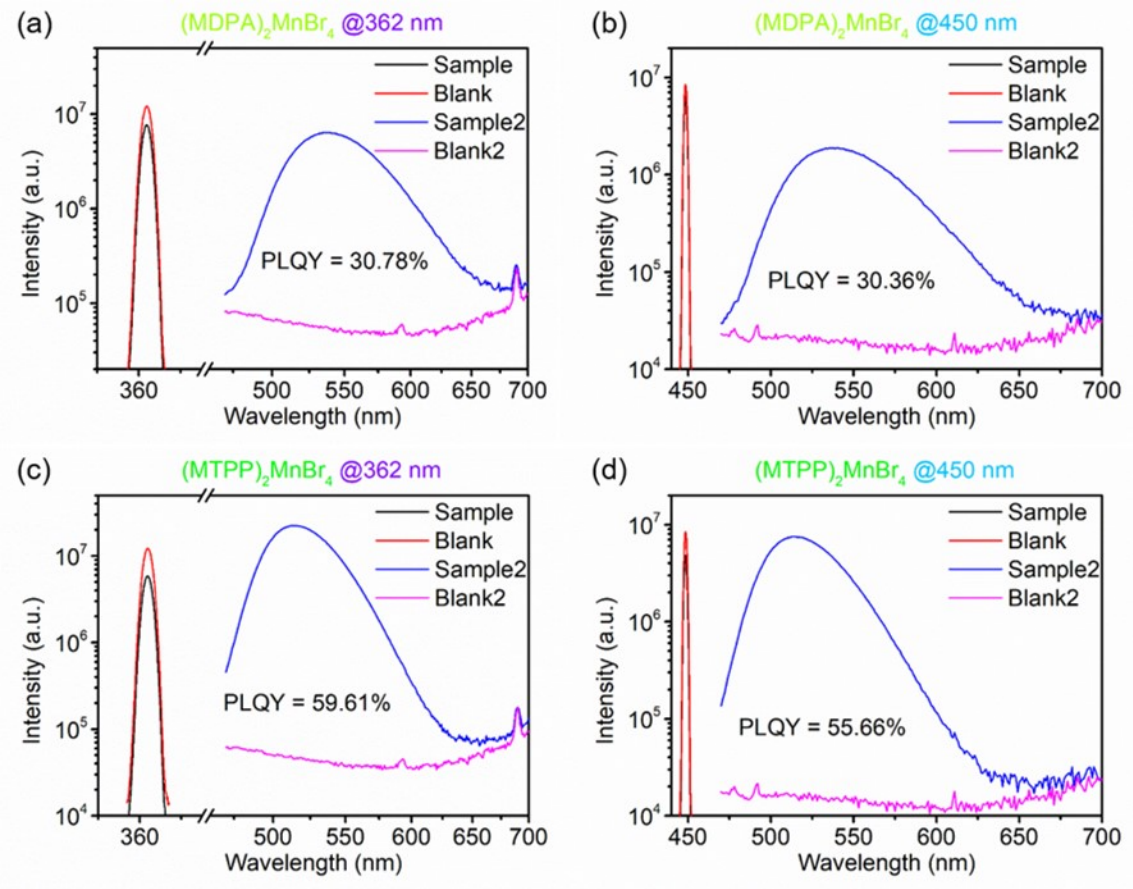

Figure S5. PLQY experimental data of (a) (b) $(MDPA)_2MnBr_4$, and (c) (d) $(MTPP)_2MnBr_4$.

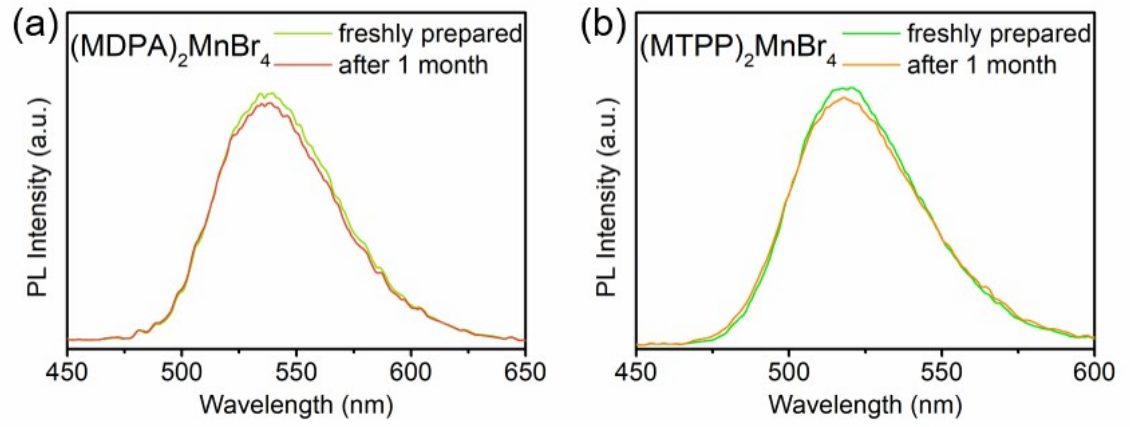

Figure S6. Comparison of the PL spectra of the as-prepared **1** (a) and **2** (b) and the ones of samples exposed in the air for 1 month.

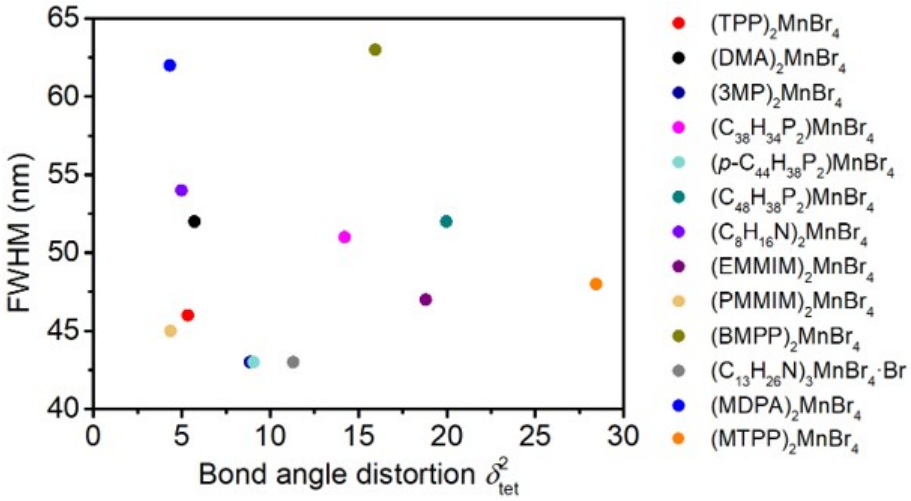

Figure S7. Relationship between the fwhm values and the bond angle distortion degree (δ^2_{tet}) in 0D Mn(II) tetrabromide hybrids.

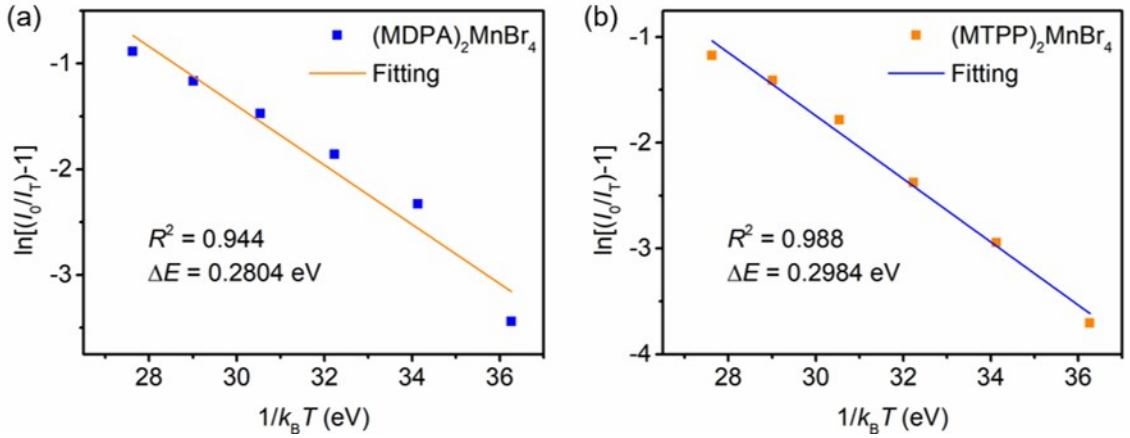

Figure S8. The thermal activation energy ΔE of (a) $(MDPA)_2MnBr_4$ and (b) $(MTPP)_2MnBr_4$ analyzed by using the Arrhenius equation.

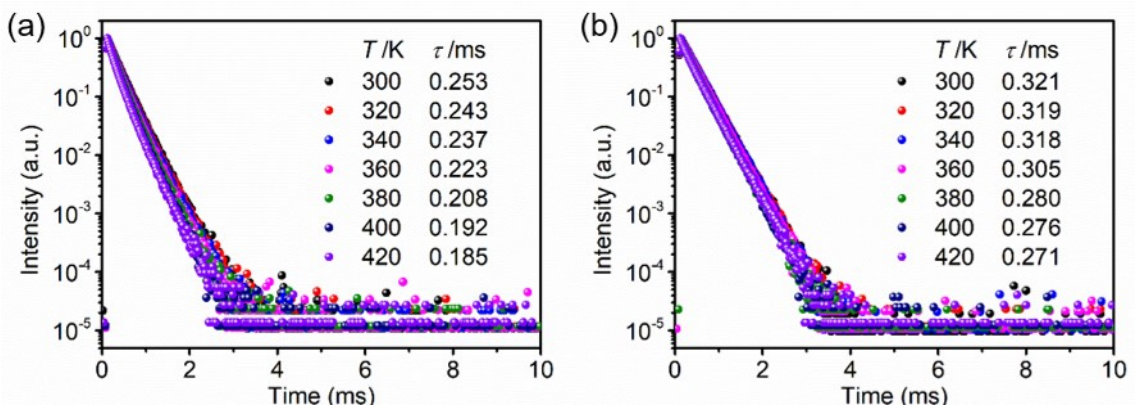

Figure S9. Temperature-dependent PL decay curves and lifetimes of (a) $(MDPA)_2MnBr_4$ and (b) $(MTPP)_2MnBr_4$.

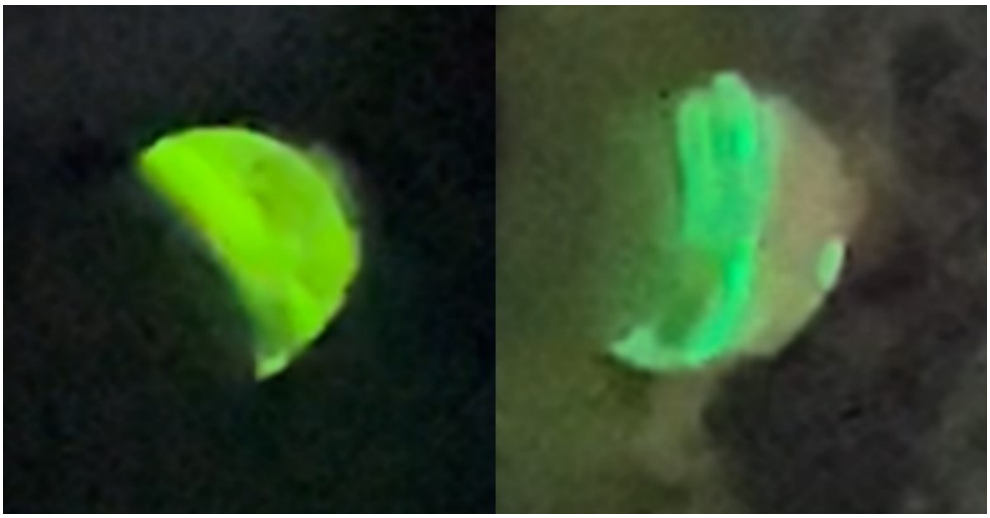

Figure S10. Photographs of the TL light captured from crystals of $(MDPA)_2MnBr_4$ (left) and $(MTPP)_2MnBr_4$ (right) upon grinding with a glass rod at ambient conditions.